Fractal Pattern Formation in Anodic Bonding of Pyrex Glass/Al/Si

Yu-Qun Hu[1], Ya-Pu Zhao[*1] , Tong-Xi Yu[2]

1. State Key Laboratory of Nonlinear Mechanics (LNM), Institute of Mechanics, Chinese Academy of Sciences, Beijing 100190, China

2. Department of Mechanical Engineering, Hong Kong University of Science and Technology, Clear Water Bay, Kowloon, Hong Kong SAR, China

Abstract

Anodic bonding of Pyrex glass/Al/Si is an important bonding technique in micro/nanoelectromechanical systems (MEMS/NEMS) industry. The anodic bonding of Pyrex 7740 glass/Aluminum film/Silicon is completed at the temperature from 300 °C to 375 °C with a bonding voltage between 150 V and 450 V. The fractal patterns are formed in the intermediate Al thin film. This pattern has the fractal dimension of the typical two-dimensional diffusion-limited aggregation (2D DLA) process, and the fractal dimension is around 1.7. The fractal patterns consist of Al and Si crystalline grains, and their occurrences are due to the limited diffusion, aggregation, and crystallization of Si and Al atoms in the intermediate Al layers. The formation of the fractal pattern is helpful to enhance the bonding strength between the Pyrex 7740 glass and the aluminum thin film coated on the crystal silicon substrates.

Keywords: Fractal pattern; DLA; Anodic bonding; Aluminum interlayer; MEMS

1. Introduction

Anodic bonding has been an effective and important process to bond some of metals, alloys or semiconductors to conductive glasses in the field of micro/nanoelectromechanical systems (MEMS /NEMS). Anodic bonding was first presented by Wallis and Pomerantz in 1969 [1] and is also known as electrostatic bonding, field-assisted bonding or Mallory bonding [2].

Compared to other techniques, anodic bonding is a highly promising method for joining certain metals or semiconductors to alkali-ion-conductive glasses at a relative low temperature [3]. Its main advantage is that, with the help of an electric field, a strong bond could be acquired at a relative low temperature of bonding [4]. The bonding temperature is usually less than the softening or melting points of the materials of the bonding pairs. Bonding at low temperature and voltage will be helpful to prevent the metal leads and integrated circuits in MEMS devices from degradation. On the other hand, the reduced bonding temperature also minimizes the thermal stress due to the large variation of temperature in the bonding process. There exist many perspective applications of this straightforward and reliable bonding technique, especially in connecting, packaging and hermetic sealing of more complex micro/nano structures and integrated micro circuits in MEMS/NEMS devices.

Anodic bonding is a complex physico-chemical process. In the process, bonding pairs are firstly brought into close contact. When the temperature goes up to bonding temperature, a direct current (DC) voltage can be applied for a certain time. Figure 1 is a schematic of anodic bonding between Pyrex 7740 glass and aluminum film coated on crystalline silicon. In order to bond the pairs successfully, the conductive glass must be connected with the

---

cathode side, and the metal, alloy or semiconductor on the anode side. Otherwise, the bonding process fails. During the bonding process, there exist the movements of mobile cations in Pyrex glass because of the electrostatic force from the applied voltage. A permanent bond is formed by anodic oxidation of the anode material at the interface [5-8].
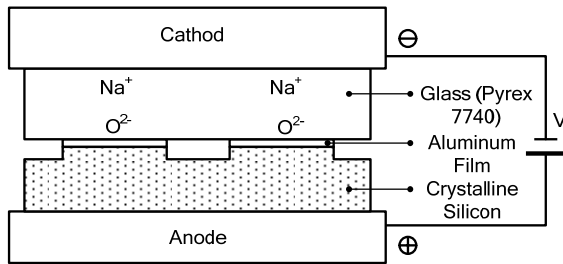

Figure 1. Schematic of anodic bonding.

Understanding the thermal-chemical-electrical-physical-mechanical coupled complex evolution process of the interface during bonding is essential to obtain strong and sealed bonds [9]. Up to now, there are many studies [6, 9-18] on anodic bonding, and of them focus on the formation of intimate contact during the initial stage of bonding or the formation of a cation depletion layer by bonding various glasses to metals, alloys, or semi-conductor materials [19, 20].

To the authors' knowledge, no study has been reported to focus on the fractal patterns in the aluminum film of anodic bonding between Pyrex glass and crystalline silicon coated with aluminum thin film as an intermediate layer at a low bonding temperature and voltage. Van Helvoort et al. [9] reported some dendritic nanostructures in the glass near the bonding interface when the glass is bonded to a thick aluminum sheet, but the authors did not find any fractal pattern in their 0.5-mm-thick aluminum anode.

The anodic bonding, with metal or alloy thin films as an intermediate layer, finds many applications in the fabrication of MEMS/NEMS devices. Studies on interfacial microstructures will provide a better understanding on the bonding mechanism and joint properties.

To examine the bonding quality of anchor structures in some MEMS sensors, we have studied the anodic bonding between Pyrex 7740 glass wafer and crystalline silicon coated with aluminum thin film as an interlayer. This kind of anchor structures plays an important role in MEMS sensors (e.g. MEMS inertial micro-accelerometers, bio-MEMS [21] and MEMS micro switches [22]). The anchor acts as mechanical or electrical connecter between the movable structures and the static substrate. In our experiments of anodic bonding, we observed some fractal patterns occurred in the aluminum film.

In this work, with the help of scanning transmission electron microscopy (STEM) and Electron Back Scatter Diffraction (EBSD), we examine the fractal patterns in the intermediate aluminum film between Pyrex glass and crystalline silicon. The objective of this study is to provide a better understanding for anodic bonding mechanism at the bonding condition of relative low temperature and voltage.

2. Experimental

Squares of 12 mm ×12 mm were cut from a 500-μm-thick Pyrex 7740 glass wafer of 100 mm in diameter. The chemical composition of the material includes 80.8 Mol% SiO_2, 12.0 Mol% B_2O_3, 4.2 Mol% Na_2O, 2.0 Mol% Al_2O_3, 0.6 Mol% K_2O, 0.2 Mol% MgO, and 0.2 Mol% CaO [23]. Si wafers of 100 mm in diameter (double-side polished; p-type; wafer surface plane, (100)), were patterned with 4 mm × 4 mm squares and with 6 mm center-to-center spacing, and these squares were of 10 μm in height with a deep reactive ion etch (DRIE) process. The patterned Si wafers were coated by an ARC-12M sputtering system with pure aluminum (99.999 %) at the film thickness of 500, 950, 1500, and 2300 Å, respectively. Then these Si wafers were also diced into squares of 12 mm ×12 mm. All square samples were cleaned by standard MEMS/ CMOS process in a 100-class clean room and dried by compressed nitrogen gas. A pair of glass and well coated crystalline silicon chip was set between two stainless steel plates. These bonding sets were placed between two hotplates, which acted as plate electrodes. The glass was connected with

the cathode side. The schematic of this bonding configuration was shown in Fig. 1. The bonding was performed on an open (non-vacuum) bonder, and the temperature of bonding was varied between 300 °C and 375 °C with a bonding voltage between 150 V and 450 V. The bonding voltage was applied when the bonding temperature reached the set point. The bonding voltage lasts for 30 minutes. When the bonding was completed, each bonded sample was cooled to room temperature of 20 °C for 2 hours.

Firstly, all specimens were examined under optical microscope, and then some of the glasses were removed to expose the aluminum film for the microanalysis with energy dispersive X-ray (EDX) and EBSD. The specimens were examined in a Sirion 400NC (FEI Field Emission Gun SEM) with the EBSD system (INCA Energy and Crystal System of Oxford).

(a)   (b)

(c)   (d)
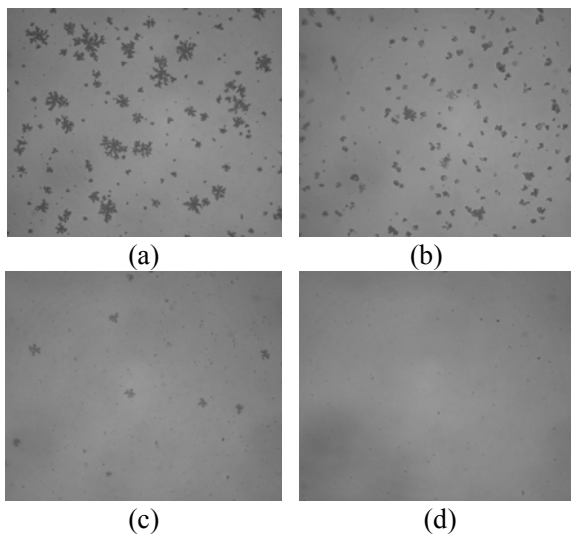
Figure 2. Fractal pattern distribution in Al film of different thickness: (a) 500 Å; (b) 950 Å; (c) 1500 Å, and (d) 2300 Å.

(a)   (b)

(c)   (d)
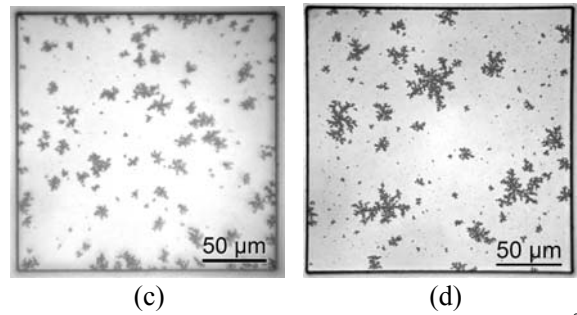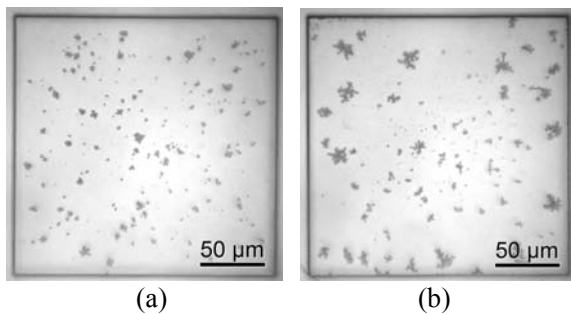
Figure 3. Fractal patterns distribution in 500 Å thick Al film at different bonding temperatures: (a) 300 °C, (b) 325 °C, (c) 350 °C, and (d) 375 °C.
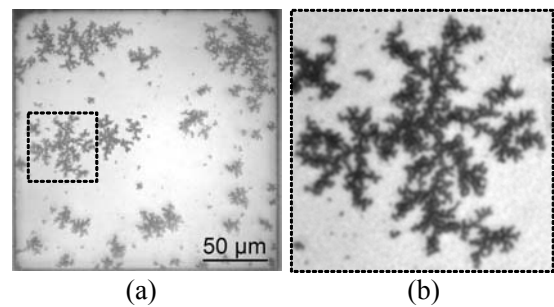

(a)   (b)

Figure 4. The typical fractal pattern 1 from 500 Å thick Al film.
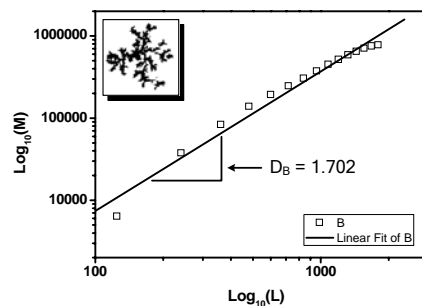

Figure 5. The typical fractal dimension is 1.702 for the pattern in Fig. 4.

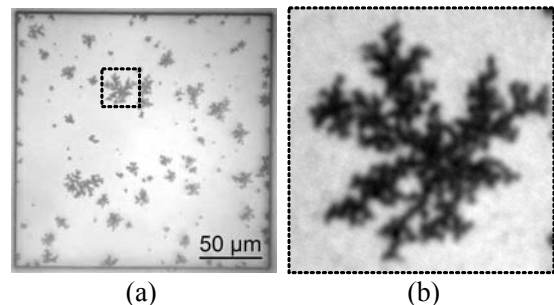(a)   (b)

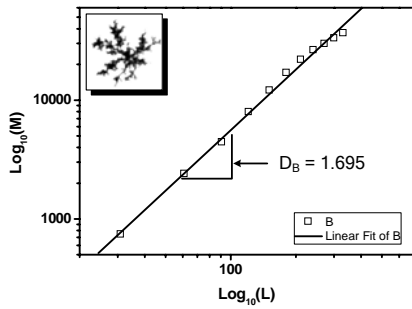Figure 6. The typical fractal pattern 2 from 500 Å thick Al film.

Figure 7. The typical fractal dimension is 1.695 for the pattern in Fig. 6.
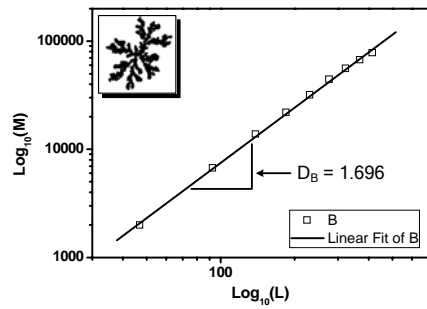

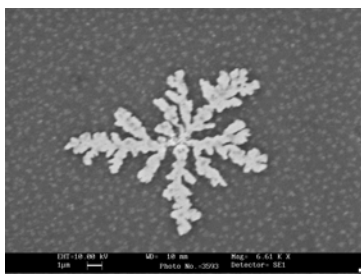Figure 11. The typical fractal dimension is 1.696 for the pattern in Fig. 10.

Figure 8. The typical fractal pattern 1 from 1500 Å thick Al film.
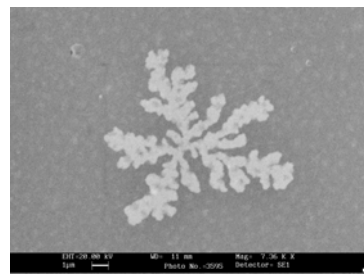

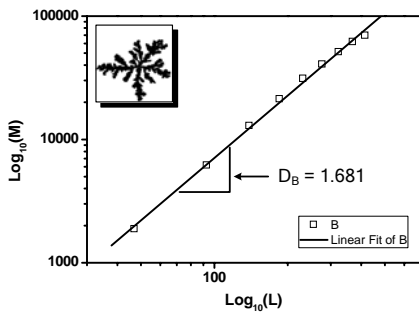Figure 12. The typical fractal pattern 3 from 1500 Å thick Al film.

Figure 9. The typical fractal dimension is 1.681 for the pattern in Fig. 8.
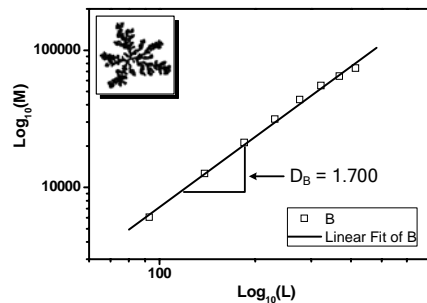

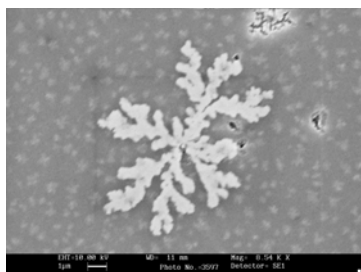Figure 13. The typical fractal dimension is 1.700 for the pattern in Fig. 12.

Figure 10. The typical fractal pattern 2 from 1500 Å thick Al film.
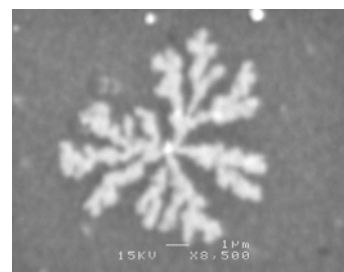

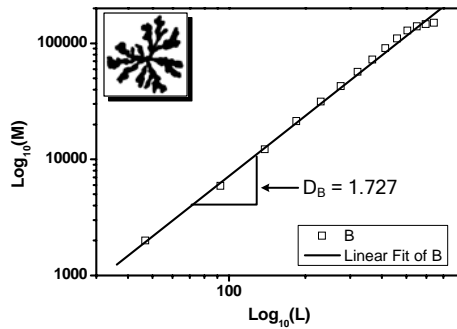Figure 14. The typical fractal pattern 4 from 1500 Å thick Al film.

Figure 15. The typical fractal dimension is 1.727 for the pattern in Fig. 14.

The EBSD results of the fractal patterns are shown in Figs. 16 and 17.
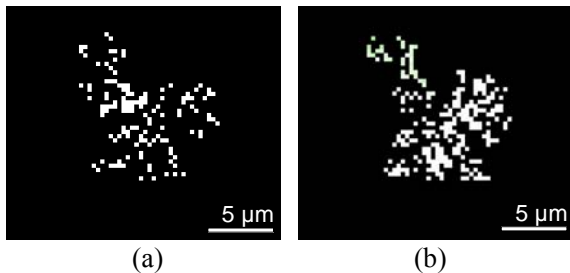

(a)   (b)

Figure 16. The distribution of crystalline grains in the fractal pattern: (a) crystalline Al, and (b) crystalline Si.
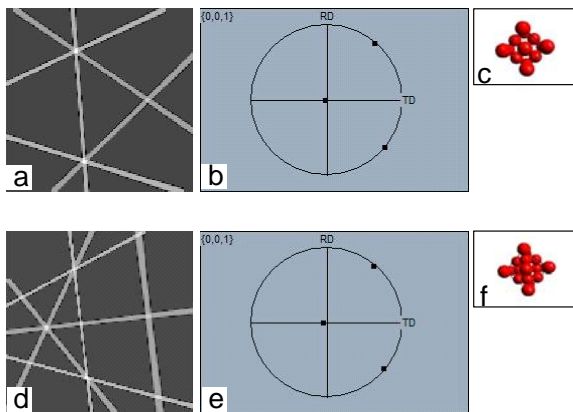

Figure 17. The orientation of the crystalline grains in the fractal patterns.

3. Results and discussion

3.1. Results

With the optical microscope, many fractal patterns were found in the intermediate aluminum film and the size of the patterns increases with the thickness of Al film, as shown in Fig. 2.

Figure 3 shows that the fractal pattern size increases with the bonding temperature.

The fractal patterns in the aluminum film have the characteristics of two-dimensional Diffusion-Limited Aggregation (DLA) model [24, 25]. The typical fractal patterns in Fig. 4 to Fig. 15 are analyzed and their fractal dimensions are calculated by sand-box method [26].

3.2. Discussion

The simplest method for determining the fractal dimension of an object is termed as sand-box method [27]. In Figs. 5, 7, 9, 11, 13, and 15, L is the side length of a square placed over a digital representation of the fractal pattern, and M is the mass of the fractal pattern contained within the square. A number of squares of increasing L are placed concentrically over the initial square and the larger the square, the more mass of fractal pattern it contains. When the mass M was plotted as a function of the length L, a power law relation can be obtained as

$$M = CL^{D_B}, \qquad (1)$$

where D_B is the fractal dimension and C is a constant.

The experimental results demonstrate that the fractal patterns in the intermediate aluminum film have the typical dimension of two-dimensional (2D) DLA process, and their fractal dimension is around 1.7, as listed in table 1.

Some fractal patterns were analyzed with the EDX and EBSD systems of INCA. The microanalyses show that the fractal patterns are full of the crystalline grains of Aluminum and Silicon. In Fig. 16, figure (a) is the distribution of the Aluminum crystalline grains, and (b) is of the Silicon's in the same fractal pattern.

Figure 17 presents the orientation of the crystalline grains in the fractal patterns. The Kikuchi lines for Al and Si are shown in Fig. 17 (a) and (d) respectively, and Figs.17 (b) and (e) are the pole figures. The Figs.17 (c) and (f) are the schematics of the orientations of Al and Si

grains, and show both of Al and Si crystalline grains have the same orientation {0,0,1} as the crystal silicon substrate.

The formation of fractal patterns in the intermediate Al film in the process of anodic bonding is due to the limited diffusion and aggregation of Si atoms in the Al film. These diffused Si atoms mainly originate from the following chemical reaction,
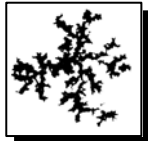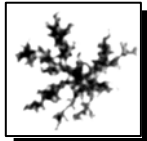
$$4Al + 3SiO_2 = 2Al_2O_3 + 3Si.$$
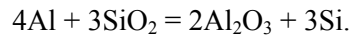
When the temperature is above 300°C, there exists a chemical reaction between the Al and SiO_2 [28]. The silicon dioxides were occurred before the aluminum sputtering process of the silicon wafer due to the slightly oxidizing of silicon wafer on its exposed surface.

For the Al film of thin enough, the fractal patterns run through the span of the whole thickness of the film, and bond with the substrate and glass. The strength of chemical bond is 799.6 ± 13.4 kcal/mol for Si-O, 511 ± 3 kcal/mol for Al-O, and 325 ± 7 kcal/mol for Si-Si [29]. Therefore, the formation of the fractal pattern improves the bonding strength between the Pyrex glass and the aluminum thin film coated on the silicon substrate.

Table 1. The typical fractal dimensions of the fractal patterns in the Al films.

Thickness of Al: 500 Å		Thickness of Al: 1500 Å			
$D_B = 1.702$	$D_B = 1.695$	$D_B = 1.681$	$D_B = 1.696$	$D_B = 1.700$	$D_B = 1.727$

4. Conclusion

The formation of the fractal patterns in the process of anodic bonding is due to the limited diffusion, aggregation, and crystallization of Si and Al atoms in the intermediate Al film. These fractal patterns have the fractal dimension of 2D DLA process, and their fractal dimension is around 1.7.

The fractal patterns in the intermediate Al film consist of Al and Si crystalline grains, which have the same orientation as the crystal silicon substrates.

The formation of the fractal patterns improves the bonding strength between the Pyrex 7740 glass and the intermediate Al layer coated on the crystal silicon substrate.

Acknowledgments

References

[1] Wallis G, Pomerantz DI. Field assisted glass-metal sealing. *Journal of Applied Physics*. 1969; 40(10): 3946-3949.

[2] Knowles KM, van Helvoort ATJ. Anodic bonding. *International Materials Review*s. 2006; 51(5): 273-311.

[3] Xing Q, Sasaki G, Fukunaga H. Interfacial microstructure of anodic-bonded Al/glass. *Journal of Materials Science: Materials in Electronics*. 2002; 13(2): 83-88.

[4] van Elp J, Giesen PTM, van der Velde JJ.

Anodic bonding using the low expansion glass ceramic Zerodur. *Journal of Vacuum Science and Technology B*. 2005; 23(1): 96-98.

[5] Veenstra TT, Berenschot JW, Gardeniers JGE, Sanders RGP, Elwenspoek MC, van den Berg A. Use of selective anodic bonding to create micropump chambers with virtually no dead volume. *Journal of the Electrochemical Society*. 2001; 148(2): G68-G72.

[6] Nitzsche P, Lange K, Schmidt B, Grigull S, Kreissig U, Thomas B, Herzog K. Ion drift processes in pyrex-type alkali-borosilicate glass during anodic bonding. J*ournal of the Electrochemical Society*. 1998; 145(5): 1755-1762.

[7] Mack S, Baumann H, Gösele U, Werner H, Schlögl R. Analysis of bonding related gas enclosure in micro machined cavities sealed by silicon wafer bonding. *Journal of the Electrochemical Society*. 1997; 144(3): 1106-1111.

[8] van Helvoort ATJ, Knowles KM, Fernie JA. Characterization of cation depletion in Pyrex during electrostatic bonding. *Journal of the Electrochemical Society*. 2003; 150(10): G624-G629.

[9] van Helvoort ATJ, Knowles KM, Fernie JA. Nanostructures at electrostatic bond interfaces. *Journal of the American Ceramic Society*. 2003; 86(10): 1773-1776.

[10] Anthony TR. Anodic bonding of imperfect surfaces. *Journal of Applied Physics*. 1983; 54(5): 2419-2428.

[11] Albaugh KB, Rasmussen DH. Rate-Processes During Anodic Bonding. *Journal of the American Ceramic Society*. 1992; 75(10): 2644-2648.

[12] Lee TMH, Lee DHY, Liaw CYN, Lao AIK, Hsing IM. Detailed characterization of anodic bonding process between glass and thin-film coated silicon substrates. *Sensors and Actuators A: Physical*. 2000; 86(1-2): 103-107.

[13] Morsy MA, Ikeuchi K, Ushio M, Abe H. Mechanism of enlargement of intimately contacted area in anodic bonding of Kovar alloy to borosilicate glass. *Materials Transactions JIM*. 1996; 37(9): 1511-1517.

[14] Borom MP. Electron-microprobe study of field-assisted bonding of glasses to metals. *Journal of the American Ceramic Society*. 1973; 56(5): 254-257.

[15] Carlson DE, Hang KW, Stockdale GF. Ion depletion of glass at a blocking anode -- 1, 2. *Journal of the American Ceramic Society*. 1974; 57(7): 291-300.

[16] Schmidt B, Nitzsche P, Grigull S, Kreissig U, Thomas B, Herzog K, Lange K. In situ investigation of ion drift processes in glass during anodic bonding. *Sensors and Actuators A: Physical*. 1998; 67(1-3): 191-198.

[17] Morsy MA, Ikeuchi K, Takahashi M, Ushio M. Microstructure of glass/metal interface of anodically-bonded joint. Pine Mountain, GA, United States: ASM International; 1998. pp. 251-256.

[18] van Helvoort ATJ, Knowles KM, Boothroyd CB, Fernie JA. Transmission electron microscopy of silicon-Pyrex electrostatic bonds. In: Aindow M, Kiely CJ, editors. Electron Microscopy and Analysis 2001. Bristol: IOP Publishing Ltd, 2001. pp. 341-344.

[19] Tudryn C, Schweizer S, Hopkins R, Hobbs L, Garratt-Reed AJ. Characterization of Si and CVD SiC to glass anodic bonding using tem and stem analysis. *Journal of the Electrochemical Society*. 2005; 152(4): E131-E134.

[20] Ko WH, Suminto JT, Yeh GJ. Bonding techniques for microsensors. Cleveland, OH, USA: Elsevier, Amsterdam, Netherlands; 1985. pp. 41-61.

[21] Dai W, Zhao Y-P. The nonlinear phenomena of thin polydimethylsiloxane (PDMS) films in electrowetting. *International Journal of Nonlinear Sciences and Numerical Simulation*. 2007; 8(4): 519-526.

[22] Lin WH, Zhao Y-P. Pull-in instability of micro-switch actuators: Model review. *International Journal of Nonlinear Sciences and Numerical Simulatio*n. 2008; 9(2): 175-183.

[23] Shelby JE. Effect of radiation on the physical properties of borosilicate glasses. *Journal of Applied Physics*. 1980; 51(5):

2561-2565.

[24] Witten TA, Sander LM. Diffusion-limited aggregation. *Physical Review B*. 1983; 27(9): 5686-5697.

[25] Witten Jr TA, Sander LM. Diffusion-limited aggregation, a kinetic critical phenomenon. *Physical Review Letters*. 1981; 47(19): 1400-1403.

[26] Forrest SR, Witten TA. Long-range correlations in smoke-particle aggregates. *Journal of Physics A*. 1979; 12(5): L109-L117.

[27] Russell SW, Li J, Mayer JW. In situ observation of fractal growth during a-Si crystallization in a Cu3Si matrix. *Journal of Applied Physics*. 1991; 70(9): 5153- 5155.

[28] Chou NJ, Eldridge JM. Effects of material and processing parameters on the dielectric strength of thermally grown SiO$_2$ films. *Journal of the Electrochemical Society*. 1970; 117(10): 1287-1293.

[29] Lide DR. Handbook of Chemistry and Physics. Boca Raton, FL: CRC Press, 2005.